blood®
Plenary Paper

MYELOID NEOPLASIA

RUNX1 isoform disequilibrium promotes the development of trisomy 21–associated myeloid leukemia

Sofia Gialesaki,[1,*] Daniela Bräuer-Hartmann,[2,*] Hasan Issa,[3] Raj Bhayadia,[3] Oriol Alejo-Valle,[2] Lonneke Verboon,[3] Anna-Lena Schmell,[3] Stephanie Laszig,[3] Enikő Regényi,[2,4] Konstantin Schuschel,[3] Maurice Labuhn,[1] Michelle Ng,[2] Robert Winkler,[3] Christian Ihling,[5] Andrea Sinz,[5] Markus Glaß,[6] Stefan Hüttelmaier,[6] Sören Matzk,[4] Lena Schmid,[1] Farina Josepha Strüwe,[1] Sofie-Katrin Kadel,[1] Dirk Reinhardt,[7] Marie-Laure Yaspo,[4] Dirk Heckl,[2,†] and Jan-Henning Klusmann[3,8,9,†]

[1]Pediatric Hematology and Oncology, Hannover Medical School, Hannover, Germany; [2]Pediatric Hematology and Oncology, Martin Luther University Halle-Wittenberg, Halle, Germany; [3]Department of Pediatrics, Goethe University Frankfurt, Frankfurt am Main, Germany; [4]Max Planck Institute for Molecular Genetics, Berlin, Germany; [5]Department of Pharmaceutical Chemistry and Bioanalytics, Institute of Pharmacy, Martin Luther University Halle-Wittenberg, Halle, Germany; [6]Institute of Molecular Medicine, Martin Luther University Halle-Wittenberg, Halle, Germany; [7]Pediatric Hematology and Oncology, Pediatrics III, University Hospital Essen, Essen, Germany; [8]Frankfurt Cancer Institute, Goethe University, Frankfurt am Main, Germany; and [9]German Cancer Consortium (DKTK), Partner Site Frankfurt/Mainz and German Cancer Research Center (DKFZ), Heidelberg, Germany

KEY POINTS

- ***RUNX1* isoform disequilibrium toward *RUNX1A* and its interaction with MYC:MAX are key in the pathogenesis of trisomy 21–associated ML.**
- **Restoration of RUNX1A:RUNX1C equilibrium and pharmacological interference with MYC:MAX dimerization reverses the oncogenic phenotype.**

Gain of chromosome 21 (Hsa21) is among the most frequent aneuploidies in leukemia. However, it remains unclear how partial or complete amplifications of Hsa21 promote leukemogenesis and why children with Down syndrome (DS) (ie, trisomy 21) are particularly at risk of leukemia development. Here, we propose that *RUNX1* isoform disequilibrium with *RUNX1A* bias is key to DS-associated myeloid leukemia (ML-DS). Starting with Hsa21-focused CRISPR–CRISPR-associated protein 9 screens, we uncovered a strong and specific *RUNX1* dependency in ML-DS cells. Expression of the *RUNX1A* isoform is elevated in patients with ML-DS, and mechanistic studies using murine ML-DS models and patient-derived xenografts revealed that excess RUNX1A synergizes with the pathognomonic *Gata1s* mutation during leukemogenesis by displacing RUNX1C from its endogenous binding sites and inducing oncogenic programs in complex with the MYC cofactor MAX. These effects were reversed by restoring the RUNX1A:RUNX1C equilibrium in patient-derived xenografts in vitro and in vivo. Moreover, pharmacological interference with MYC:MAX dimerization using MYCi361 exerted strong antileukemic effects. Thus, our study highlights the importance of alternative splicing in leukemogenesis, even on a background of aneuploidy, and paves the way for the development of specific and targeted therapies for ML-DS, as well as for other leukemias with Hsa21 aneuploidy or *RUNX1* isoform disequilibrium.

Introduction

Major multiomic efforts have mapped the cytogenetic, mutational, and epigenetic landscape of many cancers, including acute myeloid leukemia (AML).[1,2] Subsequent functional studies involving disease modeling in mice or in human cells have pointed toward complex cooperation between common fusion oncogenes and recurrently mutated genes during disease initiation and progression. However, the contribution of aneuploidy to oncogenesis remains poorly understood[3] because of context-dependent effects, technical challenges, and a lack of appropriate models. Gain of chromosome 21 (Hsa21), one of the most frequent numerical alterations in leukemia,[4,5] is no exception.

Myeloid leukemia associated with Down syndrome (ML-DS) and its preleukemic antecedent, transient abnormal myelopoiesis (TAM), are excellent paradigms for studying leukemic progression associated with trisomy 21. TAM is caused by a single genetic mutation in the transcription factor GATA1 in trisomic fetal stem and/or progenitor cells, which causes the exclusive expression of a shorter isoform known as GATA1s.[6] We, and others, have shed light on the additional mutational events that are required for progression to overt ML-DS,[7,8] however, far less is known about the role of trisomy 21 in the development of the TAM/ML-DS disease phenotype. A critical region has been identified on Hsa21 that mediates the expansion of early hematopoietic progenitors observed in patients with DS[9-11] and

Downloaded from http://ashpublications.org/blood/article-pdf/141/10/1105/2037408/blood_bld-2022-017619-main.pdf by guest on 25 September 2023

several Hsa21 genes, such as *ERG*,[12,13] *DYRK1A*,[14] *CHAF1B*,[15] and microRNA 125b (miR-125b),[16,17] have been postulated to play a role in leukemogenesis. In contrast, Ts65dn mice that are trisomic for 104 orthologs of Hsa21 genes do not fully recapitulate the human phenotype in association with *GATA1s*,[18] and the postulated factors are either located outside of the critical region, not overexpressed in trisomic fetal progenitor cells,[11] or lack full leukemic potential in humans when combined with mutated *GATA1s*.[14,19,20]

The transcription factor RUNX1, which is essential for the establishment of definitive hematopoiesis,[21-23] has attracted considerable attention as a candidate Hsa21 oncogene. Although RUNX1 has been extensively studied in leukemia development,[24,25] its expression is reduced in trisomic fetal progenitor cells[11] and its trisomy is dispensable for myeloproliferative disease in elderly Ts65dn mice.[24] Despite initial hints pointing toward differential roles for alternatively spliced *RUNX1* isoforms in ML-DS,[26] studies, to date, have not accounted for the fact that *RUNX1* is transcribed from 2 distinct promoters and undergoes alternative splicing, giving rise to 3 main isoforms with diverse effects on hematopoiesis[27]: *RUNX1C*, transcribed from the P1 promoter, is the most abundant isoform in definitive hematopoiesis. *RUNX1A* and *RUNX1B*, both transcribed from the P2 promoter, are differentially expressed throughout hematopoietic differentiation.[28-30] Interestingly, because of the lack of a splice acceptor site in an isoform-specific exon, mice do not express *RUNX1A*, the short *RUNX1* isoform that lacks the transactivation domain, underlining important species-specific differences[31] and contributing, in part, to the incomplete understanding of isoform-specific roles for RUNX1.

In this study, we systematically investigated protein-coding genes on Hsa21 for dependency in ML-DS and found that disequilibrium of the *RUNX1* isoforms, specifically excess *RUNX1A*, is key to trisomy 21–associated leukemogenesis.

Methods

Reagents and resources

Supplemental Table 1, available on the *Blood* website, contains a list of all relevant reagents.

Patient samples

Samples from pediatric patients with AML were collected from patients enrolled in the AML Berlin-Frankfurt-Münster treatment protocols for children and adolescents. Written, informed consent was obtained from all patients and custodians in accordance with the Declaration of Helsinki and local laws and regulations, and the study was approved by the institutional review boards of all participating centers. For details, refer to supplemental Table 2.

Animal studies

All animal experiments were performed according to protocols approved by the local authorities (Niedersächsisches Landesamt für Verbraucherschutz und Lebensmittelsicherheit, Landesverwaltungsamt Sachsen-Anhalt, and Regierungspräsidium Darmstadt). The animals were maintained under pathogen-free conditions.

Statistical analysis

Statistical evaluation was performed using the Student *t* test, the Mann-Whitney *U* test, and 1-way or 2-way analysis of variance. The Kaplan-Meier method and log-rank tests were used to estimate overall survival and to compare differences between survival curves, respectively. All data are presented as mean ± standard deviation. Calculations were performed using GraphPad Prism version 8/9 (STATCON). All statistical tests and sample numbers are disclosed in the respective figure legends/supplemental tables.

Additional detailed methods can be found in the supplemental Methods.

Results

CRISPR-Cas9 screen reveals RUNX1 dependency in ML-DS

To identify potential oncogenes on Hsa21 that contribute to the pathogenesis of TAM and ML-DS, we generated a lentiviral CRISPR–CRISPR-associated protein 9 (CRISPR-Cas9) library (1090 single-guide RNA [sgRNA]) targeting the 218 annotated coding genes on Hsa21 and performed a dropout screen in the ML-DS cell line CMK, as well as in the erythroleukemia cell line K562 (Figure 1A). We identified 19 genes specifically required for the survival of CMK cells (Figure 1B; supplemental Table 3). Interestingly, we observed a strong depletion of *RUNX1*-targeting sgRNAs in CMK but not in K562 cells (Figure 1B-C). Subsequent flow cytometry–based depletion assays using individual sgRNAs found *RUNX1* to be the most specific ML-DS dependency in our screen, with the sgRNAs' impact on cell survival corresponding to RUNX1 knockdown levels (Figure 1C; supplemental Figure 1A-D). These results were recapitulated in vitro in stable Cas9-expressing blasts derived from patients with ML-DS and in vivo by fluorescence-based competitive transplantation assays (Figure 1C-E; supplemental Figure 1E-G; supplemental Table 2).

Considering that former studies have disputed the role of *RUNX1* in TAM/ML-DS pathogenesis, and given that Bourquin et al hypothesized that alternatively spliced *RUNX1* isoforms may lead the reduced expression of RUNX1 targets in ML-DS,[11,24,26] we wondered whether deregulation of the *RUNX1* isoforms, rather than altered overall expression, might underlie its dependency phenotype in ML-DS cells. Nanopore full-length RNA sequencing (RNA-seq) revealed that the main isoforms, *RUNX1A*, *RUNX1B*, and *RUNX1C*, are predominant in TAM and ML-DS (Figure 1F). Thus, we further quantified the expression of these 3 isoforms in healthy hematopoietic cells (hematopoietic stem and progenitor cells [HSPCs], erythrocytes, megakaryocytes, granulocytes, and monocytes) and TAM/ML-DS blasts. *RUNX1C* is the predominant isoform in all cell types, but ML-DS and trisomy 21 samples presented with elevated expression of the *RUNX1A* isoform, resulting in a significantly higher *RUNX1A:RUNX1B/C* ratio compared with HSPCs or terminally differentiated cells (Figure 1G; supplemental Figure 1H-K).

Notably, trisomy 21 is associated with an elevated *RUNX1A:RUNX1B/C* ratio, as determined by comparing fetal trisomy 21 and nontrisomic $CD34^+$ HSPCs (supplemental Figure 1H-I). Interestingly, this imbalance can be induced by elevated levels

Downloaded from http://ashpublications.org/blood/article-pdf/141/10/1105/2037408/blood_bld-2022-017619-main.pdf by guest on 25 September 2023

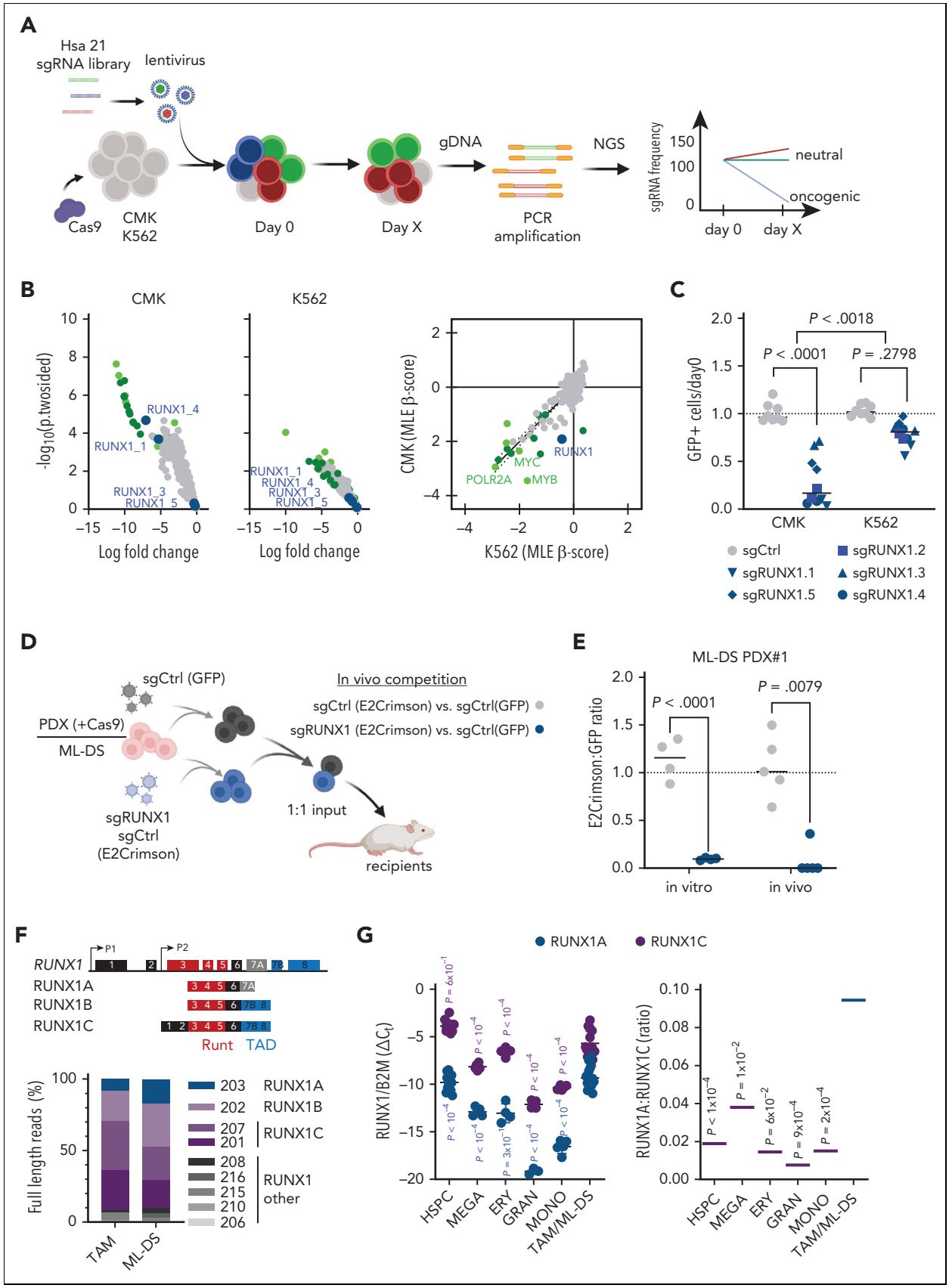

Figure 1. CRISPR-Cas9 screen reveals *RUNX1* dependency in ML-DS. (A) Schema of the high-throughput Hsa21 CRISPR-Cas9 in vitro screen. (B) Dot plots showing the $\log_{10}$ fold change and $-\log_{10}$ (*P* 2-sided) of the Hsa21 sgRNAs in CMK (left), K562 (middle), and CMK + K562 (right; maximum likelihood estimation [MLE] β score) cell lines. Dark green dots represent highly depleting sgRNAs in CMK cells that also deplete in K562s. Light green dots represent positive controls (*MYB*, *MYC*, *ACTB*, *SF3B3*, *RPL9*,

Downloaded from http://ashpublications.org/blood/article-pdf/141/10/1105/2037408/blood_bld-2022-017619-main.pdf by guest on 25 September 2023

of the splicing factor subunit U2AF1, which is encoded by chromosome 21 (supplemental Figure 2A). Moreover, GATA1s' ability to regulate *RUNX1* isoforms appears to be impaired compared with full-length GATA1; it shows reduced occupancy at the RUNX1 P1 und P2 promoter regions in *Gata1s*–fetal liver cells (FLCs) (supplemental Figure 2B-D) and causes higher *RUNX1A* levels in CRISPR-Cas9–edited human megakaryocytic/erythroid precursors cultured in vitro compared with wild-type controls (supplemental Figure 2E). Induced expression of *GATA1* and *GATA1s* in K562 cells activated transcription from the P2 promoter, leading to increased *RUNX1A* and *RUNX1B* expression, whereas *RUNX1C* transcription from the P1 promoter was enhanced by *GATA1* but repressed by *GATA1s* (supplemental Figure 2F). Altogether, these data suggest a mechanism in which trisomy 21 and *GATA1s* synergize to amplify *RUNX1* isoform imbalance.

Thus, our CRISPR-Cas9 screen of Hsa21 genes and subsequent *RUNX1* isoform expression analyses in patient samples suggest that *RUNX1* isoform disequilibrium and *RUNX1A* bias contribute to the pathogenesis of TAM and ML-DS.

Increased RUNX1A:RUNX1C ratio induces malignant ML-DS phenotype

To probe the functional relevance of unbalanced *RUNX1* isoform expression in TAM and ML-DS development, we modulated the *RUNX1A:RUNX1C* ratio in fetal and neonatal CD34$^+$ HSPCs of human origin and in patient-derived ML-DS blasts (supplemental Figure 3A). Methylcellulose-based colony-forming unit assays showed the sustained growth of *RUNX1A*-expressing CD34$^+$ HSPCs, as evidenced by increased replating capacity (Figure 2A). In culture conditions that promote megakaryocytic differentiation, *RUNX1A* expression induced the expansion of CD34$^+$ immature cells and blocked their differentiation to CD41$^+$/CD61$^+$CD42b$^+$ megakaryocytes (Figure 2B-C; supplemental Figure 3B), effects that were more pronounced in fetal cells and that we confirmed in collagen-based megakaryocytic colony-forming unit assays (supplemental Figure 3C). To better understand the effects of *RUNX1A* and *RUNX1C* on lineage fate decision, we also cultured CD34$^+$ HSPCs in conditions allowing for differentiation along the erythroid as well as megakaryocytic lineages. *RUNX1C* and *RUNX1A* conferred a lineage bias toward megakaryopoiesis (CD41$^+$/CD235a$^-$) over erythropoiesis (CD41$^-$/CD235a$^+$) in neonatal CD34$^+$ HSPCs. *RUNX1A* halted cells in an undifferentiated CD117$^+$ stage (supplemental Figure 3D-E).

Importantly, restoring the *RUNX1A:RUNX1C* equilibrium through *RUNX1C* expression in patient-derived ML-DS blasts (supplemental Figure 3A) halted proliferation and accelerated differentiation, as indicated by loss of CD117 and gain of CD33 and CD41 expression (Figure 2D-F). Inversely, further increasing the expression of *RUNX1A* conferred a mild growth advantage in ML-DS blasts and an increase in the fraction of cells with an immature phenotype (CD33$^+$CD117$^+$ or CD41$^+$CD42b$^-$CD117$^+$ myeloid/megakaryocytic blasts; Figure 2D-F). Lastly, we evaluated restoration of the *RUNX1A:RUNX1C* ratio in vivo through fluorescence-based competitive transplantation assays using 2 patient-derived xenografts from patients with ML-DS (Figure 2G). In both cases, *RUNX1C*-expressing leukemic blasts were significantly diminished in the bone marrow of recipient mice at the experimental end point, whereas *RUNX1A*-expressing leukemic blasts were unchanged compared with control-transduced blasts (Figure 2H).

In summary, these experiments in primary human cells depict a landscape of perturbed differentiation and accelerated proliferation guided by *RUNX1A*. Our data further demonstrate that restoring *RUNX1A:RUNX1C* equilibrium can overcome differentiation arrest in ML-DS blasts, leading to their depletion.

RUNX1A synergizes with *Gata1s* in the leukemic transformation of FLCs

Because TAM occurs in utero, implying a fetal origin for this disease, we employed a murine FLC-based in vitro model to study the oncogenic potential of *RUNX1* isoform imbalance in concert with mutated *Gata1s* (supplemental Figure 3A).[7] Notably, mice do not express the *RUNX1A* isoform,[31] underlining important species-specific differences that could explain the inability of previous DS mouse models to recapitulate the human TAM/ML-DS phenotype.[18,32] Combined lentiviral transduction of Cas9-knockin FLCs with *RUNX1A* and a sgRNA targeting exon 2 of *Gata1*, thereby introducing *Gata1s* mutations, indeed resulted in a robust hyperproliferative phenotype (Figure 3A; 4140-fold) compared with cells transduced with a combination of a nontargeting control sgRNA and an empty vector (EV). Individually, *Gata1s* (sgGata1 + EV) and *RUNX1A* expression (control sgRNA + *RUNX1A*) also enhanced growth (Figure 3A; 366-fold and 140-fold, respectively), but the effect was less pronounced than in combination, suggesting synergy between *Gata1s* and *RUNX1A*. Inversely, ectopic expression of *RUNX1C* or *RUNX1B* alone or in combination with *Gata1s* mutations resulted in a growth disadvantage (Figure 3A; supplemental Figure 4A). We note that none of the other Hsa21 candidate genes selected from our sgRNA dropout screen produced a synergistic hyperproliferative phenotype with *Gata1s* (supplemental Figure 4B). Immunophenotypically, the hyperproliferative *RUNX1A Gata1s*-FLCs were mainly CD117$^+$CD41$^+$ and partially CD71$^+$Ter119$^+$ (Figure 3B), corresponding to megakaryocytic progenitors with erythroid features, a hallmark of TAM/ML-DS. The expression of erythroid

Figure 1 (continued) and *POLR2A*). Blue dots represent sgRNAs targeting *RUNX1*. (C) Dot plot showing the number of sgRNA-transduced (control sgRNA [sgCtrl] and sgRUNX1.1-1.5 indicated by shape) CMK and K562 cells (with stable Cas9 expression) after 14 days of culture, normalized to day 0 (n = 2 per sgRNA, 2-tailed unpaired *t* test). (D) Experimental setup for evaluating *RUNX1* knockout in vivo. ML-DS blasts (with stable Cas9 expression) were transduced with sgRUNX1 (E2Crimson$^+$ and sgRUNX1.1) or a sgCtrl (E2Crimson$^+$) and mixed 1:1 with sgCtrl-transduced blasts (GFP$^+$), before transplantation into sublethally irradiated recipient mice. (E) Dot plot showing the ratio of E2Crimson$^+$ to green fluorescent protein–positive (GFP$^+$) cells after 12 days of culture, normalized to day 0 (left; n = 4, 2-tailed unpaired *t* test) and in the bone marrow of mice euthanized 6 to 8 weeks after transplantation (right; n = 5, Mann Whitney *U* test). (F) Schematic representation of the human *RUNX1* genomic locus (top) and the 3 main *RUNX1* transcript isoforms (bottom; not to scale). Functional exons encoding the DNA-binding domain (Runt; red) and transactivation domain (TAD; blue) are indicated. Bar graph showing *RUNX1* isoform distribution (Oxford Nanopore sequencing) in polyA$^+$-enriched RNA samples from TAM and ML-DS samples. (G) Expression of *RUNX1A* and *RUNX1C* isoforms normalized to the expression of β2-microglobulin (*B2M*) (left graph; 2-way analysis of variance [ANOVA]) and *RUNX1A* to *RUNX1C* ratios (right graph; 1-way ANOVA) in CD34$^+$ HSPCs, erythrocytes, megakaryocytes, granulocytes, and monocytes isolated from healthy donors, as well as in leukemic blasts from patients with TAM/ML-DS. gDNA, genomic DNA; NGS, next-generation sequencing; PCR, polymerase chain reaction.

Downloaded from http://ashpublications.org/blood/article-pdf/141/10/1105/2037408/blood_bld-2022-017619-main.pdf by guest on 25 September 2023

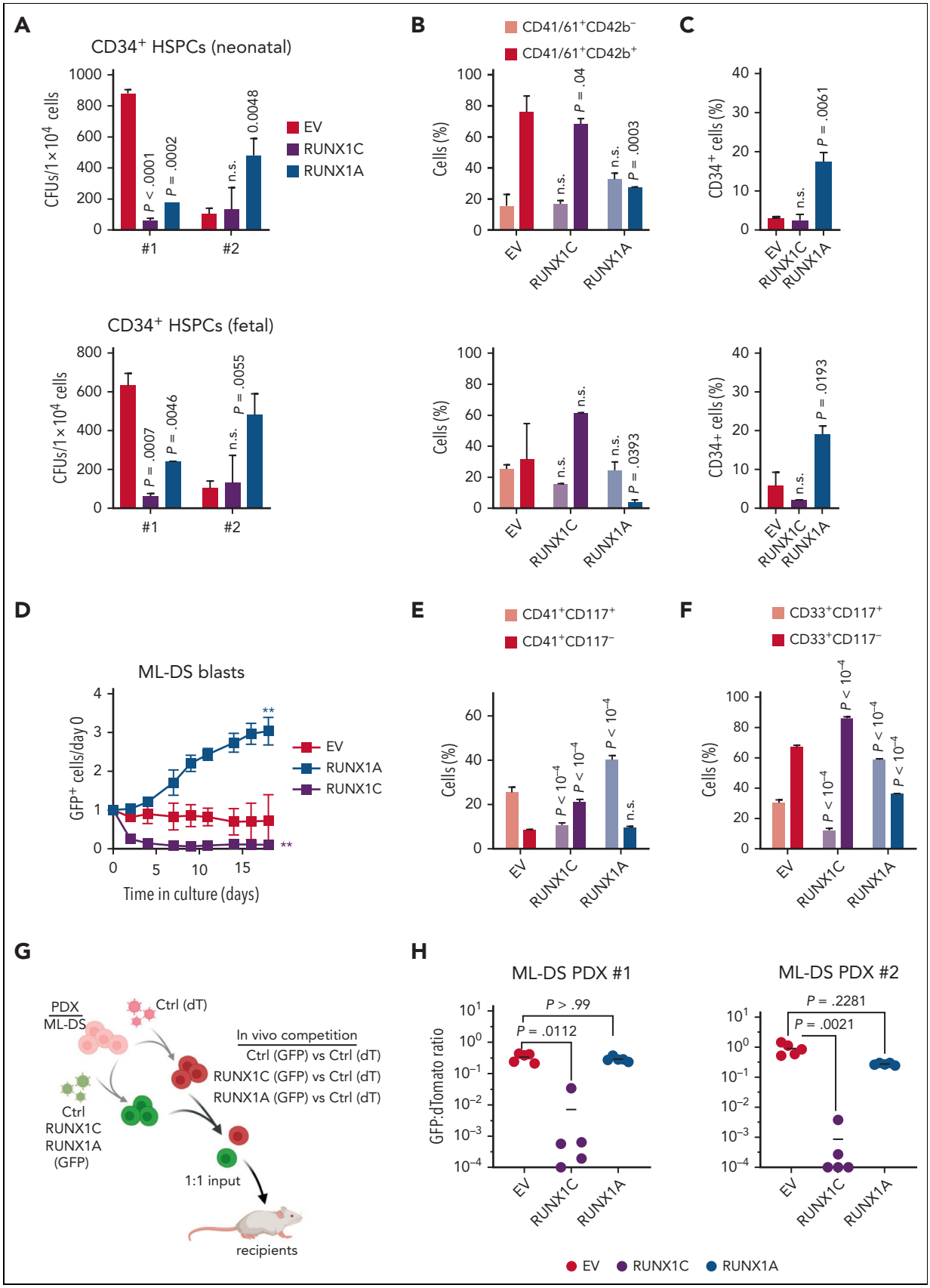

Figure 2. Increased RUNX1A:RUNX1C ratio induces malignant ML-DS phenotype. (A-C) Neonatal (top) and fetal (bottom) CD34$^+$ HSPCs were lentivirally transduced with *RUNX1A*, *RUNX1C*, or EV control. (A) Colonies after plating CD34$^+$ HSPCs from 2 independent donors in methylcellulose-based colony-forming unit (CFU) assays (mean ± standard deviation [SD], n = 2, 1-way ANOVA). Percentage of immature (CD41$^+$CD61$^+$/CD42$^-$) and mature megakaryocytes (CD41$^+$CD61$^+$/CD42$^+$) (B) and immature CD34$^+$

Downloaded from http://ashpublications.org/blood/article-pdf/141/10/1105/2037408/blood_bld-2022-017619-main.pdf by guest on 25 September 2023

Downloaded from http://ashpublications.org/blood/article-pdf/141/10/1105/2037408/blood_bld-2022-017619-main.pdf by guest on 25 September 2023

protein complexes in the presence of GATA1. We found that both GATA1 and GATA1s interact with RUNX1C, as previously described.[46] However, neither GATA1 nor GATA1s appear to interact with RUNX1A (Figure 4D). Thus, our proteomic data suggest an altered protein interaction network, which may contribute to the TAM/ML-DS–specific phenotype of RUNX1A in *GATA1*-mutated cells.

RUNX1A affects gene regulation by displacing endogenous RUNX1C

To further interrogate the RUNX1A-centered protein interaction network and determine the consequences of its inability to form a complex with GATA1 or GATA1s, we performed CUT&RUN on endogenous GATA1s and RUNX1C (using a C-terminal antibody that does not recognize exogenous RUNX1A) in *Gata1s*-FLC with or without exogenous expression of doxycycline-inducible HA-tagged RUNX1A or RUNX1C (Figure 5A; supplemental Figure 6A)[47]. We found that 33% of the promoter or enhancer regions occupied by endogenous RUNX1C were also occupied by HA-RUNX1A, and that half (52%) of the RUNX1C/RUNX1A-occupied regulatory regions were cobound by GATA1s (Figure 5B; supplemental Table 6), corroborating the known GATA1-RUNX1 interplay in transcriptional regulation.[48]

Unsupervised clustering of peaks at regulatory regions bound by endogenous RUNX1C, GATA1, and HA-RUNX1A revealed 3 clusters (Figure 5C). De novo motif discovery uncovered an enrichment of RUNX family motifs in clusters 1 and 3, whereas GATA family motifs were most abundant in cluster 2 (supplemental Figure 6B-C). Importantly, we observed a global reduction of endogenous RUNX1 occupancy upon HA-RUNX1A expression across all clusters (Figure 5D; supplemental Figure 6D; supplemental Table 6). Consistent with our protein-protein interaction studies, GATA1s binding increased globally upon expression of HA-RUNX1C, compared with HA-RUNX1A and the EV control (Figure 5D; supplemental Figure 6E).

Interestingly, most of the genes in the 3 CUT&RUN clusters were upregulated upon HA-RUNX1A expression (67.6% to 81.5%) (supplemental Figure 6C). Transcription factor motif analysis of peaks in the promoter regions of differentially expressed genes revealed an overrepresentation of the MYC-coactivation factor E2F, as well as of single MYC, MAX, and MYC:MAX dimeric motifs (Figure 5E; supplemental Table 7). The median distance between the RUNX1 and MYC:MAX binding motifs (under HA-RUNX1A peaks) was 298 base pairs. Among the RUNX1A-induced genes with MAX or MYC:MAX binding motifs in their promoter regions are *Max dimerization protein 1* (*Mxd1* [*Mad1*]), *MYC target 1* (*Myct1*), known oncogenic drivers such as *Lyl1* and *Malat1*, as well as the megakaryocyte gene *Itga2b* (CD41), all of which were repressed by RUNX1C in RNA-seq experiments (Figure 5F; supplemental Figure 6F-H). These data are consistent with our comparative transcriptomic analyses in *Gata1s*-FLCs that uncovered that the activation of MYC and E2F targets by GATA1s and RUNX1A results in a synergistic induction of proliferation and an immature phenotype, whereas the opposite was true for *RUNX1C* (Figure 3C-E).

Taken together, our proteomic and genomic analyses imply that RUNX1A interferes with normal RUNX1C function by displacing it from target gene promoters. Instead, RUNX1A interacts with the MYC cofactor MAX and induces an MYC- and E2F-driven expression program. The concerted alteration of normal megakaryocytic progenitor gene expression programs through GATA1s and RUNX1A leads to malignant transformation in these cells via the upregulation of oncogenic gene expression programs and the perturbation of RUNX1C-regulated differentiation programs, respectively.

Targeting MYC:MAX dimerization as a therapeutic approach for ML-DS

Finally, we investigated the role of the MYC cofactor MAX, which we hypothesized to be central in the synergy between GATA1s and RUNX1A, during leukemia pathogenesis. Short hairpin RNA–mediated knock down and sgRNA-mediated knock out of *MAX* inhibited the growth of CMK cells in vitro (supplemental Figure 7A-B). These findings were confirmed in murine *RUNX1A Gata1s*-FLCs and in ML-DS blasts derived from 2 patients (supplemental Figure 7C-F). Normal $CD34^+$ HSPCs showed only a mild growth impairment upon *MAX* depletion (supplemental Figure 7G-H). Importantly, pharmacological disruption of MYC:MAX dimerization using the MYC inhibitor MYCi361[49] caused apoptotic cell death in *RUNX1A Gata1s*-FLCs and in CMK and K562 cells, which are *MYC*-dependent (Figure 1B), in a dose-dependent manner (Figure 6A; supplemental Figure 8A-B). Accordingly, MYCi361 also induced apoptosis and partial differentiation in ML-DS blasts derived from 3 patients, with median lethal concentration (50% inhibitory concentration [IC_{50}]) values of 2.09 μM, 2.63 μM, and 3.82 μM, respectively (Figure 6B; supplemental Figure 8C). Similarly, blasts derived from patients with non-DS acute megakaryoblastic leukemia (AMKL) or *KMT2Ar*, 2 other AML subgroups that have elevated *RUNX1A:RUNX1C* ratios

Figure 3 (continued) immunophenotype is indicated in the corresponding gates. Data from 3 replicates ± SD are shown. (C-D) Bar graphs showing NESs of significantly upregulated or downregulated gene sets associated with differentiation and oncogenic cellular programs, in *Gata1s*- (sgGata1s + EV, orange), *RUNX1A*- (sgCtrl + *RUNX1A*, blue), and *Gata1s*- and *RUNX1A*- (sgGATA1s + *RUNX1A*, red) murine FLCs compared with sgCtrl + EV control FLCs. This analysis highlights the unique and synergistic functional features of *Gata1s* and *RUNX1A*. *False discovery rate (FDR) $q < .25$; **FDR $q < .05$. (E) Bar graph showing NESs of significantly upregulated or downregulated gene sets in (red) *Gata1s* + *RUNX1A*– and (green) *Gata1s* + *RUNX1C*–expressing FLCs compared with control sgCtrl + EV FLCs. This analysis highlights the contrasting functional features of *RUNX1A* and *RUNX1C* on a *Gata1s* background. *FDR $q < .25$; **FDR $q < .05$. (F-H) Analysis of mice transplanted with *RUNX1A*- or EV-transduced *Gata1s*-FLCs (n = 10 per group), including comparisons of Kaplan-Meier survival curves (log-rank test) (F), spleen weights (unpaired Student *t* test) (G), and flow cytometry on bone marrow cells from the diseased mice (2-way ANOVA) (H). (I) Heat map representation of RNA-seq data, showing unsupervised hierarchical clustering on the 2824 most variable genes (SD > 1) across 5 bone marrow samples from leukemic mice and fluorescence-activated cell sorter–sorted murine fetal liver HSCs [LSK ($Lin^-Sca1^+cKit^+$), common myeloid progenitors (CMPs) ($Lin^-Sca1^-cKit^+CD34^+$ $CD16/32^{med}$), granulocyte-monocyte progenitors (GMPs) ($Lin^-Sca1^-cKit^+CD34^+$ $CD16/32^+$), and megakaryocyte-erythroid progenitors (MEPs) ($Lin^-Sca1^-cKit^+CD34^-$ $CD16/32^{low}$)]. The sample types are color coded on the bottom of the heat map and *z* scores are indicated by the legend at the top of the panel. (J) Bar graph showing NESs of significantly upregulated or downregulated gene sets in the murine leukemia samples compared with all progenitor populations. *FDR $q < .25$; **FDR $q < .05$. LT-HSCs, long-term hematopoietic stem cells.

Downloaded from http://ashpublications.org/blood/article-pdf/141/10/1105/2037408/blood_bld-2022-017619-main.pdf by guest on 25 September 2023

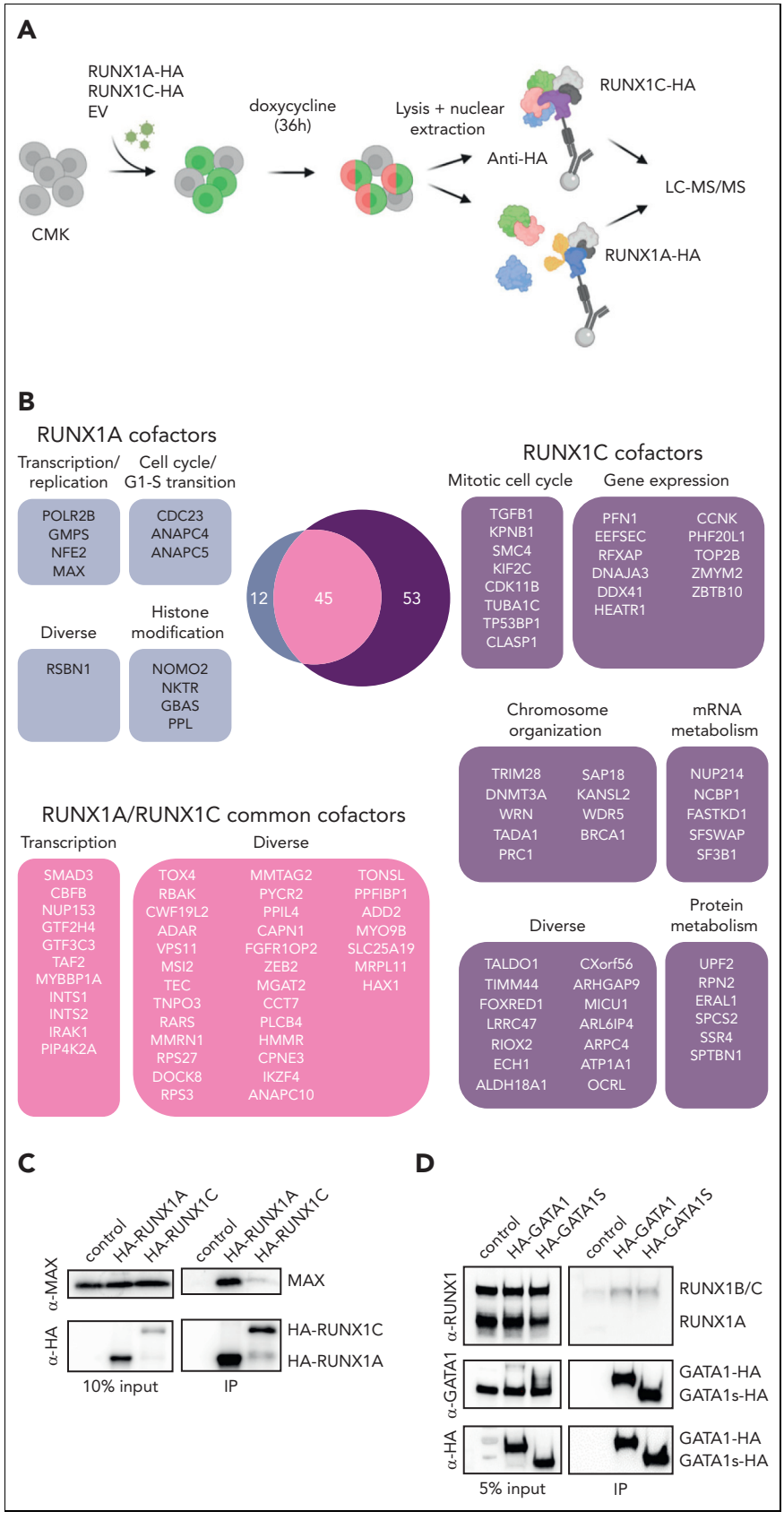

Figure 4. Distinct RUNX1A and RUNX1C protein interaction networks. (A) Experimental setup for isolating HA-RUNX1A– or HA-RUNX1C–containing protein complexes from CMK cells. (B) RUNX1A and RUNX1C complex composition in CMK cells with functional grouping. The Venn diagram shows significantly enriched interactors (log_2 fold change > 1; $P < .05$). (C) Western blot confirming coimmunoprecipitation of MAX and RUNX1A using anti-MAX and anti-RUNX1 antibodies. Representative picture of 2 independent experiments using K562 cells are shown. A 10% input was used as the loading control. (D) Western blot showing RUNX1A/C isoforms coimmunoprecipitated with doxycycline-inducible HA-tagged GATA1 and GATA1s or the EV vector. Representative pictures of 3 independent experiments using CMK cells are shown. A 5% input was used as the loading control. IP, immunoprecipitation; mRNA, messenger RNA.

Downloaded from http://ashpublications.org/blood/article-pdf/141/10/1105/2037408/blood_bld-2022-017619-main.pdf by guest on 25 September 2023

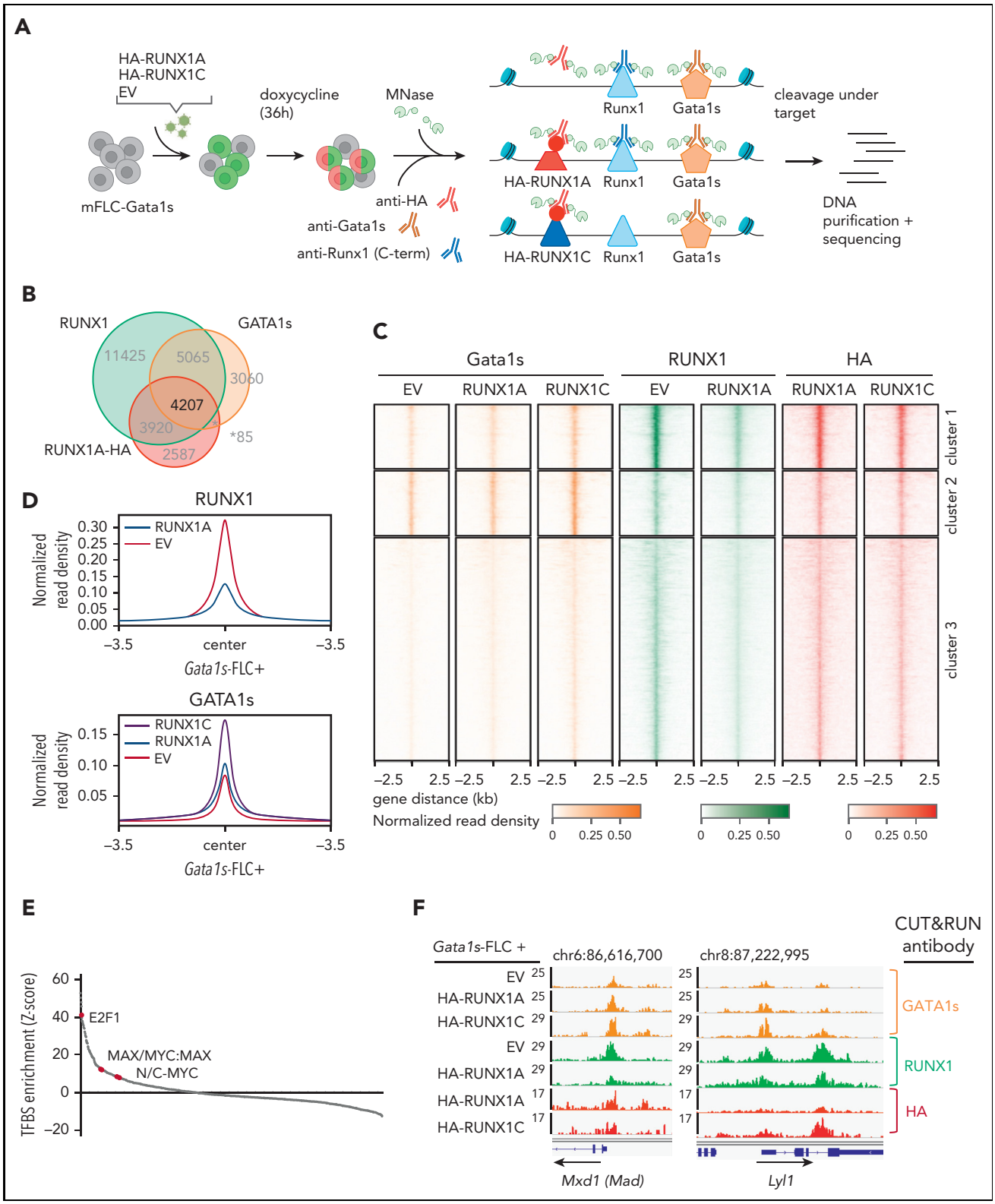

Figure 5. RUNX1A affects gene regulation by displacing endogenous RUNX1C. (A) Experimental setup of CUT&RUN on murine *Gata1s*-FLCs after doxycycline-induced expression of HA-RUNX1A/RUNX1C. CUT&RUN was performed using anti-HA, anti-RUNX1(C-term), and anti-GATA1 antibodies. Peaks were called by SEACR[47] using EV control cells as background. Data represent 1 experiment. (B) Venn diagram showing the number of genomic regions bound by endogenous RUNX1, endogenous GATA1s, and/or HA-RUNX1A after HA-RUNX1A overexpression. (C) Heat maps depicting the colocalization of endogenous GATA1s (orange, left), endogenous RUNX1 (green, middle), and HA-RUNX1A/-RUNX1C (red, right) signals after doxycycline-induced HA-RUNX1A or HA-RUNX1C expression in Gata1s-FLCs. EV-transduced cells were used as a control. Regions ±2.5 kilobases (kb) of the peak center are shown. Binding intensities are represented as normalized reads per kilobase of transcript per million reads mapped values (bars below the blots). (D) Binding intensities (normalized read density) of RUNX1 (left) and GATA1s (right), in EV control and doxycycline-induced HA-RUNX1A and HA-RUNX1C expressing cells. (E) Transcription factor motif enrichment analysis under RUNX1 peaks, at the promoter regions of genes that are differentially expressed upon

Downloaded from http://ashpublications.org/blood/article-pdf/141/10/1105/2037408/blood_bld-2022-017619-main.pdf by guest on 25 September 2023

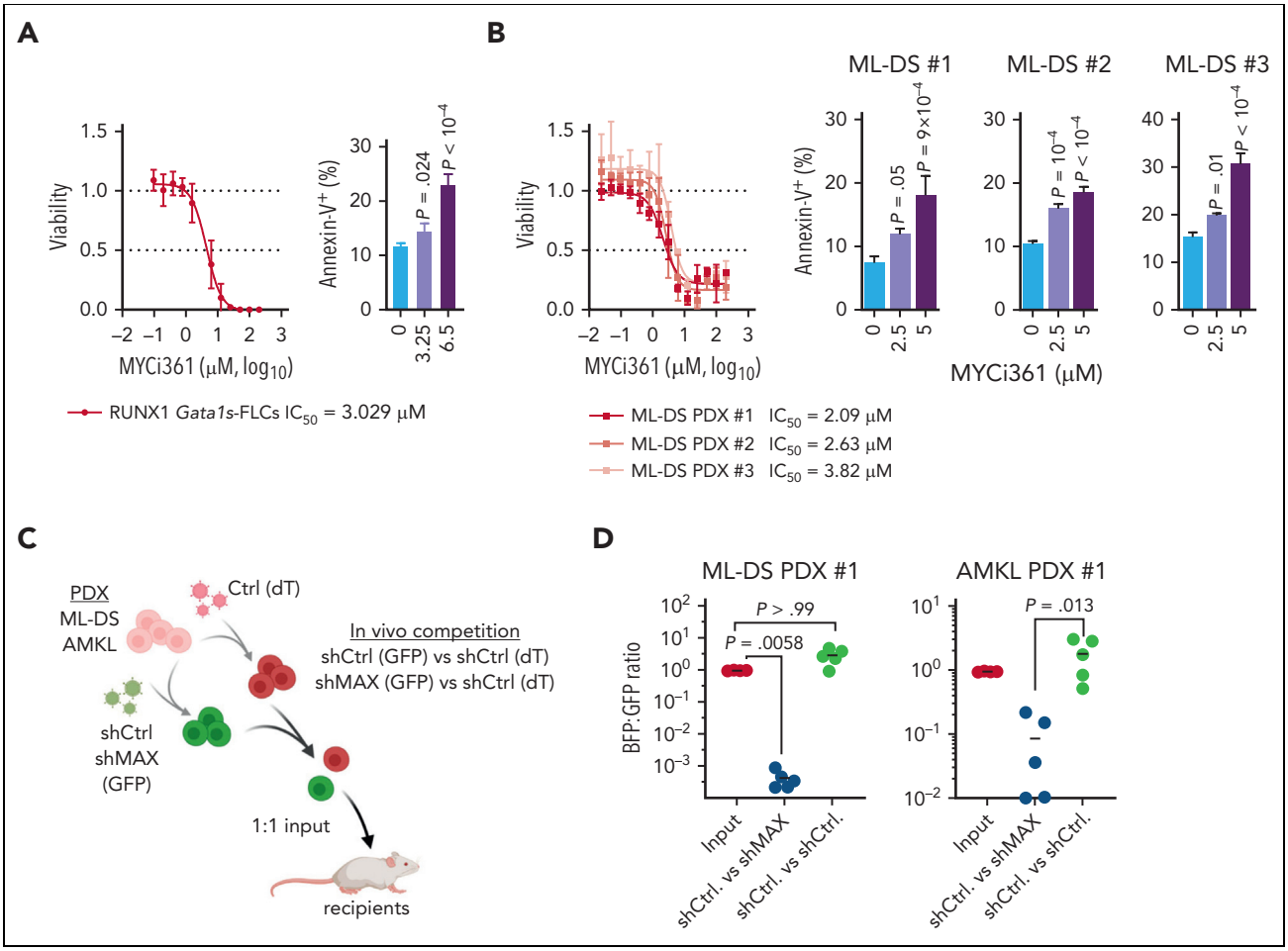

Figure 6. Interfering with MYC:MAX dimerization as a therapeutic strategy. Dose response curves for MYC:MAX dimerization inhibitor MYCi361 in *Gata1s*-FLC cells (A, left) and in ML-DS blasts derived from 3 patients (B, left) 24 hours after treatment in vitro. Corresponding IC_{50} values are depicted below the graphs. Bar graphs showing the percentage of annexin V^+ cells after treatment with the indicated doses of MYCi361 compared with the dimethyl sulfoxide control in *Gata1s*-FLCs (A, right) and in ML-DS blasts (B, right); data represented as mean ± SD (n = 3, 1-way ANOVA). (C) Experimental setup for evaluating MAX dependence in ML-DS and AMKL cells in vivo. ML-DS or AMKL blasts derived from 2 patients were transduced with short hairpin *MAX* (*shMAX*) (GFP^+) or short hairpin control (shCtrl) (GFP^+) and mixed 1:1 with shCtrl-transduced blasts ($dTomato^+$), before transplantation into sublethally irradiated recipient mice. (D) Ratio of GFP^+ to $dTomato^+$ cells in the bone marrow of mice euthanized 4 to 8 weeks after transplantation (n = 5, Kruskal-Wallis test).

(supplemental Figure 1H-K) also showed good responses with partial differentiation and median IC_{50} values between 3.9 and 4.32 μM and from 3.9 to 5.88 μM, respectively (supplemental Figure 8D-H). Normal $CD34^+$ HSPCs from 2 donors had IC_{50} values of 7.291 μM and 7.168 μM, respectively (supplemental Figure 8I-K), outlining a therapeutic window. Lastly, we evaluated *MAX* knockdown in vivo through fluorescence-based competitive transplantation assays using patient-derived xenografts from patients with ML-DS and AMKL (Figure 6C). In both cases, *MAX*-depleted leukemic blasts were significantly diminished in the bone marrow of recipient mice at the experimental end point (Figure 6D).

Thus, we have demonstrated that the MYC cofactor MAX is key to leukemic transformation mediated by RUNX1A and GATA1s, and that it can be therapeutically exploited.

Discussion

Aneuploidies, and in particular, partial or complete amplifications of chromosome 21, are frequent alterations in leukemia; however, their underlying pathomechanisms remain enigmatic.[3] In this study, we leveraged the model system of DS-associated TAM and ML-DS to interrogate oncogenic factors on chromosome 21 for their roles in AML pathogenesis. A CRISPR-Cas9 screen of chromosome 21 genes unexpectedly revealed *RUNX1* as an ML-DS dependency in cell lines and patient-derived blasts in vitro and in vivo, despite former controversy regarding its role in TAM and ML-DS.[3,24] Through detailed functional validation, we discovered that *RUNX1* isoform disequilibrium in the form of *RUNX1A* bias, rather than *RUNX1* gene dosage, is key to trisomy 21–associated leukemogenesis. By dissecting the consequences of *RUNX1*

Figure 5 (continued) doxycycline-induced RUNX1A expression (log_2 fold change = 1). Human promoter regions were used as background. z score intensities are shown. (F) Integrative Genomics Viewer snapshots of *Mxd1* and *Lyl1* gene promoters showing occupancy of endogenous GATA1s, RUNX1, and HA-RUNX1A/-RUNX1C in *Gata1s*-FLCs after doxycycline-induced HA-RUNX1A/HA-RUNX1C expression or in EV control–expressing cells. The tracks display coverage (reads per kilobase of transcript per million reads mapped) (left). Scale and chromosome location are shown (top).

disequilibrium in TAM/ML-DS, we showed that *RUNX1A* acts in concert with pathognomonic *GATA1s* mutations in this context, thereby blocking megakaryocytic differentiation and accelerating progenitor proliferation, effects that were reversed upon restoring the *RUNX1A*:*RUNX1C* equilibrium in murine models and patient-derived blasts in vitro and in vivo. These findings are in line with the known function of *RUNX1C* during adult hematopoiesis,[50-52] in which it regulates megakaryopoiesis by controlling the proliferation and survival of committed progenitors.[53] Thus, through the systematic interrogation of chromosome 21–encoded coding genes, our work contributes to understanding the synergy between trisomy 21 and *GATA1* mutations in ML-DS leukemogenesis. We suggest a model in which *RUNX1A*:*RUNX1C* disequilibrium in TAM and ML-DS is a consequence of the combination of trisomy 21 and *GATA1s* mutations in fetal HSPCs. Our findings have further implications for other types of leukemia with numerical or structural alterations of chromosome 21 and/or *RUNX1* isoform disequilibrium. Indeed, we also observed elevated *RUNX1A:RUNX1C* ratios in non-DS AMKL, *KMT2A*-rearranged AML, and AML with complex karyotype (supplemental Figure 1E-K). The exact mechanism leading to *RUNX1A:RUNX1C* dysregulation in trisomy 21 HSPCs remains an open question. One hypothesis is that altered transcriptional regulation by GATA1s and elevated levels of the Hsa21-encoded splicing factor *U2AF1* may combine to drive *RUNX1* isoform imbalance in TAM and ML-DS (supplemental Figure 2); different mechanisms or mutations in splicing factors may be responsible in other subtypes of AML or myelodysplastic syndromes.[54] In addition, RUNX1A might further enhance the oncogenic effect of miR-125b, another well-characterized oncogenic driver on chromosome 21.[16]

Mechanistically, we showed that the altered protein interaction network of RUNX1A (compared with RUNX1B/C) underlies its oncogenic function. RUNX1A fails to interact with GATA1 and GATA1s to control megakaryopoiesis.[46] Our proteomics analyses point toward RUNX1A's increased affinity for the MYC cofactor MAX. We propose a model in which RUNX1A, in complex with MAX, displaces RUNX1C from its endogenous binding sites where it normally recruits GATA1. Thus, RUNX1A perturbs RUNX1C:GATA1 regulated gene expression and activates MYC:MAX and E2F target genes, leading to a megakaryocytic differentiation block and acceleration of progenitor proliferation. This model would help explain the synergistic oncogenic effect of RUNX1A and GATA1s; GATA1s not only fails to repress *RUNX1A* but also E2F and MYC target genes during megakaryopoiesis,[18] suggesting a double hit on these pathways in fetal trisomy 21 HSPCs. The central role of MAX in the RUNX1A-induced phenotype was validated by genetically interfering with *MAX* expression. Importantly, the dependency of ML-DS blasts on intact MAX represents a vulnerability that can be therapeutically exploited, as we demonstrated by using the MYC:MAX dimerization inhibitor MYCi361[49] to eradicate blasts from patients with ML-DS.

Although previous studies have reported the oncogenic and overriding negative effects that RUNX1A exerts on RUNX1B,[54-58] our findings are unexpected and have general implications for basic oncology research. First, this study demonstrates that species-specific differences in isoform expression must be considered when interpreting species-specific or divergent phenotypes in mouse models. *RUNX1A* is a primate-specific isoform of *RUNX1*,[31] which may explain the inability of DS mouse models[32,59] to recapitulate the human TAM/ML-DS phenotype or the interplay of GATA1s and trisomy 21 seen in human induced pluripotent stem cells.[3,11,19,60] Second, this study underlines the importance of accounting for all isoforms when studying the oncogenic effects of a given gene and emphasizes the importance of alternative splicing in the pathogenesis of cancer. Various mutations in splicing factors have been identified in AML and MDS genomes.[61] Whether these mutations are causative for the increased RUNX1A:RUNX1B/C ratio observed in MDS[54] will need to be investigated in the future.

Overall, our study provides a general framework for interrogating the contribution of aneuploidy in oncogenesis. Given the current state of the field, in which we have a near-complete map of the cytogenetic, mutational, and epigenetic landscape of cancer, these insights will be crucial for understanding the complex cooperation between common fusion oncogenes, recurrently mutated genes, and larger amplifications or deletions during disease initiation and progression. As we have illustrated with the identification of MAX as a RUNX1A cofactor and its pharmacological inhibition, this knowledge can have direct therapeutic implications.

Acknowledgments

The authors thank D. Trono of École Polytechnique Fédérale de Lausanne, Lausanne, Switzerland, for kindly providing pMD2.G (Addgene plasmid 12259) and psPAX2 (Addgene plasmid 12260) and D. E. Zhang for sharing the *RUNX1A* complementary DNA.

This work was supported by grants from the German Research Foundation (DFG; KL-2374/1-3) (J.-H.K.), BMBF (01GM1911D myPred) (J.-H.K.), the Deutsche Krebshilfe (DKH; #109251 and #110806) (J.-H.K.), the European Research Council under the European Union's Horizon 2020 research and innovation programme (grant agreement number 714226) (J.-H.K.) and the DKH (#111743) (D.H.). S.G., M.L., F.J.S., S.-K.K., and L.S. were supported by the Hannover Biomedical Research School. J.-H.K. is a recipient of the St. Baldrick's Robert Arceci Innovations Award.

Figures and the visual abstract were created with BioRender.com.

Authorship

Contribution: S.G. and D.B.-H. performed experiments, analyzed and interpreted data, and revised the manuscript; H.I., R.B., O.A.-V., L.V., A.-L.S., S.L., M.L., C.I., L.S, F.J.S., and S.-K.K. performed experiments and analyzed data; E.R., K.S., M.G., S.M., R.W., and M.N. performed bioinformatics analysis and data interpretation and revised the manuscript; A.S., S.H., and M.-L.Y. supervised the analyses and revised the manuscript; D.R. provided patient material and data; and D.H. and J.-H.K. designed the study, analyzed and interpreted data, wrote the manuscript, and academically drove the project.

Conflict-of-interest disclosure: D.R. has advisory roles for Celgene Corporation, Novartis, bluebird bio, and Janssen and receives research funding from CLS Behring and Roche. J.-H.K. has advisory roles for bluebird bio, Novartis, Roche, and Jazz Pharmaceuticals. M.-L.Y. is partially employed by Alacris Theranostics. The remaining authors declare no competing financial interests.

ORCID profiles: D.B.-H., 0000-0001-9200-5455; A.-L.S., 0000-0003-4676-3153; M.N., 0000-0001-5113-3733; M.G., 0000-0003-2718-8907; F.J.S., 0000-0001-7712-1300; D.R., 0000-0002-7027-4483; J.-H.K., 0000-0002-1070-0727.

Downloaded from http://ashpublications.org/blood/article-pdf/141/10/1105/2037408/blood_bld-2022-017619-main.pdf by guest on 25 September 2023

Correspondence: Jan-Henning Klusmann, Department of Pediatrics, Goethe University Frankfurt, Theodor Stern Kai 7, 60590 Frankfurt, Germany; email: jan-henning.klusmann@kgu.de; and Dirk Heckl, Pediatric Hematology and Oncology, Martin Luther University Halle-Wittenberg, Ernst-Grube-Str. 40, 06120 Halle, Germany; email: dirk.heckl@uk-halle.de.

Footnotes

Submitted 29 June 2022; accepted 22 November 2022; prepublished online on *Blood* First Edition 9 December 2022. https://doi.org/10.1182/blood.2022017619.

*S.G. and D.B.-H. contributed equally to this study.

†D.H. and J.-H.K. are senior authors.

The RNA sequencing gene expression data reported in this article have been deposited in the European Nucleotide Archive (accession numbers ERS6071576-ERS6071595). The CUT&RUN data reported in this article have been deposited in the European Nucleotide Archive (accession numbers ERS5956460-ERS5956467). The mass spectrometry proteomics data reported in this article have been deposited in the ProteomeXchange Consortium via the PRIDE partner repository (data set identifier PXD030616 and 10.6019/PXD030616).

Data will be available immediately following publication, no end date, and are available on request from the corresponding authors, Jan-Henning Klusmann (jan-henning.klusmann@kgu.de) and Dirk Heckl (dirk.heckl@uk-halle.de).

The online version of this article contains a data supplement.

There is a *Blood* Commentary on this article in this issue.

The publication costs of this article were defrayed in part by page charge payment. Therefore, and solely to indicate this fact, this article is hereby marked "advertisement" in accordance with 18 USC section 1734.

Downloaded from http://ashpublications.org/blood/article-pdf/141/10/1105/2037408/blood_bld-2022-017619-main.pdf by guest on 25 September 2023

REFERENCES

1. Cancer Genome Atlas Research N, Ley TJ, Miller C, et al. Genomic and epigenomic landscapes of adult de novo acute myeloid leukemia. *N Engl J Med*. 2013;368(22):2059-2074.
2. Bolouri H, Farrar JE, Triche T Jr, et al. The molecular landscape of pediatric acute myeloid leukemia reveals recurrent structural alterations and age-specific mutational interactions. *Nat Med*. 2018;24(1):103-112.
3. Maclean GA, Menne TF, Guo G, et al. Altered hematopoiesis in trisomy 21 as revealed through in vitro differentiation of isogenic human pluripotent cells. *Proc Natl Acad Sci U S A*. 2012;109(43):17567-17572.
4. Mitelman F, Heim S, Mandahl N. Trisomy 21 in neoplastic cells. *Am J Med Genet Suppl*. 1990;7:262-266.
5. Duijf PH, Schultz N, Benezra R. Cancer cells preferentially lose small chromosomes. *Int J Cancer*. 2013;132(10):2316-2326.
6. Wechsler J, Greene M, McDevitt MA, et al. Acquired mutations in GATA1 in the megakaryoblastic leukemia of Down syndrome. *Nat Genet*. 2002;32(1):148-152.
7. Labuhn M, Perkins K, Matzk S, et al. Mechanisms of progression of myeloid preleukemia to transformed myeloid leukemia in children with Down syndrome. *Cancer Cell*. 2019;36(2):123-138.e110.
8. Yoshida K, Toki T, Okuno Y, et al. The landscape of somatic mutations in Down syndrome-related myeloid disorders. *Nat Genet*. 2013;45(11):1293-1299.
9. Gurbuxani S, Vyas P, Crispino JD. Recent insights into the mechanisms of myeloid leukemogenesis in Down syndrome. *Blood*. 2004;103(2):399-406.
10. Banno K, Omori S, Hirata K, et al. Systematic cellular disease models reveal synergistic interaction of trisomy 21 and GATA1 mutations in hematopoietic abnormalities. *Cell Rep*. 2016;15(6):1228-1241.
11. Roy A, Cowan G, Mead AJ, et al. Perturbation of fetal liver hematopoietic stem and progenitor cell development by trisomy 21. *Proc Natl Acad Sci U S A*. 2012;109(43):17579-17584.
12. Ng AP, Hyland CD, Metcalf D, et al. Trisomy of Erg is required for myeloproliferation in a mouse model of Down syndrome. *Blood*. 2010;115(19):3966-3969.
13. Birger Y, Goldberg L, Chlon TM, et al. Perturbation of fetal hematopoiesis in a mouse model of Down syndrome's transient myeloproliferative disorder. *Blood*. 2013;122(6):988-998.
14. Malinge S, Bliss-Moreau M, Kirsammer G, et al. Increased dosage of the chromosome 21 ortholog Dyrk1a promotes megakaryoblastic leukemia in a murine model of Down syndrome. *J Clin Invest*. 2012;122(3):948-962.
15. Volk A, Liang K, Suraneni P, et al. A CHAF1B-dependent molecular switch in hematopoiesis and leukemia pathogenesis. *Cancer Cell*. 2018;34(5):707-723.e707.
16. Alejo-Valle O, Weigert K, Bhayadia R, et al. The megakaryocytic transcription factor ARID3A suppresses leukemia pathogenesis. *Blood*. 2022;139(5):651-665.
17. Wagenblast E, Araujo J, Gan OI, et al. Mapping the cellular origin and early evolution of leukemia in Down syndrome. *Science*. 2021;373(6551):eabf6202.
18. Klusmann JH, Godinho FJ, Heitmann K, et al. Developmental stage-specific interplay of GATA1 and IGF signaling in fetal megakaryopoiesis and leukemogenesis. *Genes Dev*. 2010;24(15):1659-1672.
19. Chou ST, Byrska-Bishop M, Tober JM, et al. Trisomy 21-associated defects in human primitive hematopoiesis revealed through induced pluripotent stem cells. *Proc Natl Acad Sci U S A*. 2012;109(43):17573-17578.
20. Grimm J, Heckl D, Klusmann JH. Molecular mechanisms of the genetic predisposition to acute megakaryoblastic leukemia in infants with Down syndrome. *Front Oncol*. 2021;11:636633.
21. Okuda T, van Deursen J, Hiebert SW, Grosveld G, Downing JR. AML1, the target of multiple chromosomal translocations in human leukemia, is essential for normal fetal liver hematopoiesis. *Cell*. 1996;84(2):321-330.
22. Wang Q, Stacy T, Binder M, Marin-Padilla M, Sharpe AH, Speck NA. Disruption of the Cbfa2 gene causes necrosis and hemorrhaging in the central nervous system and blocks definitive hematopoiesis. *Proc Natl Acad Sci U S A*. 1996;93(8):3444-3449.
23. North TE, de Bruijn MF, Stacy T, et al. Runx1 expression marks long-term repopulating hematopoietic stem cells in the midgestation mouse embryo. *Immunity*. 2002;16(5):661-672.
24. Kirsammer G, Jilani S, Liu H, et al. Highly penetrant myeloproliferative disease in the Ts65Dn mouse model of Down syndrome. *Blood*. 2008;111(2):767-775.
25. Liu X, Zhang Q, Zhang DE, et al. Overexpression of an isoform of AML1 in acute leukemia and its potential role in leukemogenesis. *Leukemia*. 2009;23(4):739-745.
26. Bourquin JP, Subramanian A, Langebrake C, et al. Identification of distinct molecular phenotypes in acute megakaryoblastic leukemia by gene expression profiling. *Proc Natl Acad Sci U S A*. 2006;103(9):3339-3344.
27. Ghozi MC, Bernstein Y, Negreanu V, Levanon D, Groner Y. Expression of the human acute myeloid leukemia gene AML1 is regulated by two promoter regions. *Proc Natl Acad Sci U S A*. 1996;93(5):1935-1940.
28. Fujita Y, Nishimura M, Taniwaki M, Abe T, Okuda T. Identification of an alternatively spliced form of the mouse AML1/RUNX1 gene transcript AML1c and its expression in early hematopoietic development. *Biochem Biophys Res Commun*. 2001;281(5):1248-1255.

29. Sroczynska P, Lancrin C, Kouskoff V, Lacaud G. The differential activities of Runx1 promoters define milestones during embryonic hematopoiesis. *Blood*. 2009; 114(26):5279-5289.

30. Challen GA, Goodell MA. Runx1 isoforms show differential expression patterns during hematopoietic development but have similar functional effects in adult hematopoietic stem cells. *Exp Hematol*. 2010;38(5):403-416.

31. Komeno Y, Yan M, Matsuura S, et al. Runx1 exon 6-related alternative splicing isoforms differentially regulate hematopoiesis in mice. *Blood*. 2014;123(24):3760-3769.

32. Li Z, Godinho FJ, Klusmann JH, Garriga-Canut M, Yu C, Orkin SH. Developmental stage-selective effect of somatically mutated leukemogenic transcription factor GATA1. *Nat Genet*. 2005;37(6):613-619.

33. Ling T, Birger Y, Stankiewicz MJ, et al. Chromatin occupancy and epigenetic analysis reveal new insights into the function of the GATA1 N terminus in erythropoiesis. *Blood*. 2019;134(19):1619-1631.

34. Birdwell C, Fiskus W, Kadia TM, DiNardo CD, Mill CP, Bhalla KN. EVI1 dysregulation: impact on biology and therapy of myeloid malignancies. *Blood Cancer J*. 2021; 11(3):64.

35. Schwarzer A, Emmrich S, Schmidt F, et al. The non-coding RNA landscape of human hematopoiesis and leukemia. *Nat Commun*. 2017;8(1):218.

36. Emmrich S, Rasche M, Schoning J, et al. miR-99a/100~125b tricistrons regulate hematopoietic stem and progenitor cell homeostasis by shifting the balance between TGFβ and Wnt signaling. *Genes Dev*. 2014; 28(8):858-874.

37. Grinev VV, Barneh F, Ilyushonak IM, et al. RUNX1/RUNX1T1 mediates alternative splicing and reorganises the transcriptional landscape in leukemia. *Nat Commun*. 2021; 12(1):520.

38. Arkoun B, Robert E, Boudia F, et al. Stepwise GATA1 and SMC3 mutations alter megakaryocyte differentiation in a Down syndrome leukemia model. *J Clin Invest*. 2022;132(14):e156290.

39. Jutzi JS, Bogeska R, Nikoloski G, et al. MPN patients harbor recurrent truncating mutations in transcription factor NF-E2. *J Exp Med*. 2013;210(5):1003-1019.

40. Marcault C, Zhao LP, Maslah N, et al. Impact of NFE2 mutations on AML transformation and overall survival in patients with myeloproliferative neoplasms. *Blood*. 2021; 138(21):2142-2148.

41. Elagib KE, Racke FK, Mogass M, Khetawat R, Delehanty LL, Goldfarb AN. RUNX1 and GATA-1 coexpression and cooperation in megakaryocytic differentiation. *Blood*. 2003; 101(11):4333-4341.

42. Alford KA, Reinhardt K, Garnett C, et al. Analysis of GATA1 mutations in Down syndrome transient myeloproliferative disorder and myeloid leukemia. *Blood*. 2011; 118(8):2222-2238.

43. Kanezaki R, Toki T, Terui K, et al. Down syndrome and GATA1 mutations in transient abnormal myeloproliferative disorder: mutation classes correlate with progression to myeloid leukemia. *Blood*. 2010;116(22):4631-4638.

44. Crossley M, Merika M, Orkin SH. Self-association of the erythroid transcription factor GATA-1 mediated by its zinc finger domains. *Mol Cell Biol*. 1995;15(5):2448-2456.

45. Shimizu R, Trainor CD, Nishikawa K, Kobayashi M, Ohneda K, Yamamoto M. GATA-1 self-association controls erythroid development in vivo. *J Biol Chem*. 2007; 282(21):15862-15871.

46. Xu G, Kanezaki R, Toki T, et al. Physical association of the patient-specific GATA1 mutants with RUNX1 in acute megakaryoblastic leukemia accompanying Down syndrome. *Leukemia*. 2006;20(6): 1002-1008.

47. Meers MP, Tenenbaum D, Henikoff S. Peak calling by Sparse Enrichment Analysis for CUT&RUN chromatin profiling. *Epigenet Chromatin*. 2019;12(1):42.

48. Tijssen MR, Cvejic A, Joshi A, et al. Genome-wide analysis of simultaneous GATA1/2, RUNX1, FLI1, and SCL binding in megakaryocytes identifies hematopoietic regulators. *Dev Cell*. 2011;20(5):597-609.

49. Han H, Jain AD, Truica MI, et al. Small-molecule MYC inhibitors suppress tumor growth and enhance immunotherapy. *Cancer Cell*. 2019;36(5):483-497.e415.

50. Ichikawa M, Asai T, Saito T, et al. AML-1 is required for megakaryocytic maturation and lymphocytic differentiation, but not for maintenance of hematopoietic stem cells in adult hematopoiesis. *Nat Med*. 2004;10(3): 299-304.

51. Growney JD, Shigematsu H, Li Z, et al. Loss of Runx1 perturbs adult hematopoiesis and is associated with a myeloproliferative phenotype. *Blood*. 2005;106(2):494-504.

52. Senserrich J, Batsivari A, Rybtsov S, et al. Analysis of Runx1 Using induced gene ablation reveals its essential role in pre-liver HSC development and limitations of an in vivo approach. *Stem Cell Rep*. 2018;11(3): 784-794.

53. Draper JE, Sroczynska P, Leong HS, et al. Mouse RUNX1C regulates premegakaryocytic/erythroid output and maintains survival of megakaryocyte progenitors. *Blood*. 2017;130(3): 271-284.

54. Sakurai H, Harada Y, Ogata Y, et al. Overexpression of RUNX1 short isoform has an important role in the development of myelodysplastic/myeloproliferative neoplasms. *Blood Adv*. 2017;1(18): 1382-1386.

55. Tanaka T, Tanaka K, Ogawa S, et al. An acute myeloid leukemia gene, AML1, regulates hemopoietic myeloid cell differentiation and transcriptional activation antagonistically by two alternative spliced forms. *EMBO J*. 1995; 14(2):341-350.

56. Bertrand-Philippe M, Ruddell RG, Arthur MJ, Thomas J, Mungalsingh N, Mann DA. Regulation of tissue inhibitor of metalloproteinase 1 gene transcription by RUNX1 and RUNX2. *J Biol Chem*. 2004; 279(23):24530-24539.

57. Guo H, Ma O, Speck NA, Friedman AD. Runx1 deletion or dominant inhibition reduces Cebpa transcription via conserved promoter and distal enhancer sites to favor monopoiesis over granulopoiesis. *Blood*. 2012;119(19):4408-4418.

58. Ran D, Shia WJ, Lo MC, et al. RUNX1a enhances hematopoietic lineage commitment from human embryonic stem cells and inducible pluripotent stem cells. *Blood*. 2013;121(15):2882-2890.

59. Alford KA, Slender A, Vanes L, et al. Perturbed hematopoiesis in the Tc1 mouse model of Down syndrome. *Blood*. 2010; 115(14):2928-2937.

60. Byrska-Bishop M, VanDorn D, Campbell AE, et al. Pluripotent stem cells reveal erythroid-specific activities of the GATA1 N-terminus. *J Clin Invest*. 2015;125(3):993-1005.

61. Makishima H, Visconte V, Sakaguchi H, et al. Mutations in the spliceosome machinery, a novel and ubiquitous pathway in leukemogenesis. *Blood*. 2012;119(14): 3203-3210.

© 2023 by The American Society of Hematology. Licensed under Creative Commons Attribution-NonCommercial-NoDerivatives 4.0 International (CC BY-NC-ND 4.0), permitting only noncommercial, nonderivative use with attribution. All other rights reserved.

Downloaded from http://ashpublications.org/blood/article-pdf/141/10/1105/2037408/blood_bld-2022-017619-main.pdf by guest on 25 September 2023